

Catalysis Science & Technology

Accepted Manuscript

This article can be cited before page numbers have been issued, to do this please use: J. Zhang, L. Pei, J. Wang, P. Zhu, X. Gu and Z. Zheng, *Catal. Sci. Technol.*, 2020, DOI: 10.1039/C9CY02260K.



This is an Accepted Manuscript, which has been through the Royal Society of Chemistry peer review process and has been accepted for publication.

Accepted Manuscripts are published online shortly after acceptance, before technical editing, formatting and proof reading. Using this free service, authors can make their results available to the community, in citable form, before we publish the edited article. We will replace this Accepted Manuscript with the edited and formatted Advance Article as soon as it is available.

You can find more information about Accepted Manuscripts in the [Information for Authors](#).

Please note that technical editing may introduce minor changes to the text and/or graphics, which may alter content. The journal's standard [Terms & Conditions](#) and the [Ethical guidelines](#) still apply. In no event shall the Royal Society of Chemistry be held responsible for any errors or omissions in this Accepted Manuscript or any consequences arising from the use of any information it contains.

ARTICLE

Differences in Selective Reduction Mechanism of 4-Nitroacetophenone Catalysed by Rutile and Anatase Supported Ruthenium Catalysts

Received 00th January 20xx,
Accepted 00th January 20xx

DOI: 10.1039/x0xx00000x

Jin Zhang,^{ab} Linjuan Pei,^{ab} Jie Wang,^{ab} Pengqi Zhu,^{*ab} Xianmo Gu^{*a} and Zhanfeng Zheng^{*ab}

Ru/TiO₂ catalyst exhibits excellent catalytic performance for selective reduction of 4-nitroacetophenone to 4-aminoacetophenone at the normal temperature and atmospheric hydrogen. Moreover, 99.9% selectivity to 4-aminoacetophenone can be obtained over the 2.7 wt% Ru/TiO₂(anatase) catalyst even in a relatively wide temperature (55-115 °C) and time range (1-12 h). Its excellent catalytic performance is derived from the activation of H₂ on the Ru nanoparticles at atmospheric pressure and the strong interaction of nitro groups with the support surface. Additionally, Ru nanoparticles supported on different crystalline TiO₂(anatase and rutile) result in different reaction pathways for 4-nitroacetophenone. Since the Ti-Ti distance on the rutile surface is smaller than that on the anatase surface, the hydroxylamine species adsorbed on the Ti atom of rutile are more susceptible to the coupling reaction. Therefore, the Ru/TiO₂(rutile) causes a series of intermediates accumulation during the conversion process, while the Ru/TiO₂(anatase) allows the highly selective conversion of 4-nitroacetophenone to 4-aminophenone. In addition, Ru/TiO₂(anatase) can achieve chemoselective reduction of nitroaromatics to the corresponding anilines in the presence of -CN, -CHO, -COOH, especially nitroaromatics containing C=C and C≡C, indicating the excellent applicability.

Introduction

Aromatic amines are significant intermediates to dyes, pesticides, pharmaceuticals and other fine chemicals, which are generally synthesized by the reduction of nitroaromatics.¹⁻³ However, it is quite challenging to reduce the nitro group when other reducible groups are present in the same molecule.⁴⁻⁷ For instance, the selective reduction of nitro group in 4-nitroacetophenone is a key step to obtain 4-aminoacetophenone.⁸ Nevertheless, the traditional noble metals such as Pt, Rh and Ru catalysts can simultaneously reduce both nitro groups and carbonyl groups to generate undesired byproducts.^{9, 10} It is a challenge to design catalysts with selective reduction of the nitro groups while maintaining carbonyl groups unchanged. Hawkins et al. studied the selective hydrogenation of 4-nitroacetophenone with different Pt, Pd and Rh catalysts. 97% selectivity toward 4-aminoacetophenone could be obtained from the hydrogenation of 4-nitroacetophenone over the 5 wt% Pd/CaCO₃/Pb catalyst in a low hydrogen pressure.¹¹ Jackson et al. studied the selective hydrogenation of 3-nitroacetophenone and 4-nitroacetophenone with Rh/SiO₂ catalyst. It was found that the hydrogenation reaction activity of the functional group on the

Rh/SiO₂ catalyst was nitro > carbonyl > phenyl.^{9, 12} When the 4-nitroacetophenone was completely transformed, the selectivity to 4-aminoacetophenone decreased continuously with the prolonging of reaction time and/or the increase of temperature. Subsequently, Yin et al. found that the 100% selectivity to 3-aminoacetophenone was achieved at complete conversion of 3-nitroacetophenone over the 0.3 wt% Pt/TiO₂ even at high temperature.¹³ In addition, they discovered that the reduction efficiency of nitroacetophenone for Rh/TiO₂ was 16 times higher than that for Rh/SiO₂, indicating that TiO₂ as support can effectively improve the reaction activity of the catalyst.¹³ Consequently, the choice of support was crucial to prepare the catalyst. Selecting suitable supports can not only effectively promote the maximum utilization of noble metals, but also transform nonselective catalysts into highly chemoselective catalysts. Corma et al. found that Ru, which was not chemoselective for the hydrogenation of 3-nitrostyrene, can be transformed into selective catalyst through supporting it on TiO₂.¹⁴ It is well-known that there are two commonly crystalline forms of TiO₂ (rutile and anatase).^{15, 16} For the rutile surface, there was a flat profile where the 2-fold-coordinated bridging O anions were bound to the 6-fold-coordinated Ti cations and projected out of the surface plane, however, anatase surface has a sawtooth profile in which the 2-fold-coordinated O anions were bound to the 5-fold-coordinated Ti cations.^{17, 18} Therefore, there were obvious differences between rutile and anatase surface which have great influence on the catalytic performance.¹⁹⁻²² It is necessary to study the relationship between the catalytic performance of noble metals supported on

^a State Key Laboratory of Coal Conversion, Institute of Coal Chemistry, Chinese Academy of Sciences, Taiyuan 030001, China. E-mail: zfzheng@sxicc.ac.cn; guxm@sxicc.ac.cn; zhupengqi15@mails.ucas.ac.cn.

^b Center of Materials Science and Optoelectronics Engineering, University of Chinese Academy of Sciences, Beijing 100049, China.

Electronic Supplementary Information (ESI): Catalyst characterisation, catalytic performances and in situ FT-IR spectra. See DOI:10.1039/x0xx00000x

TiO₂ of differently crystalline forms and the chemoselective reduction of nitro group.

In the past century, various heterogeneous catalytic systems have been widely used in the selective reduction of the nitroaromatics.²³⁻²⁵ For the reduction process of nitroaromatics, the generally accepted reduction process was proposed by Haber in 1898.²⁶ In this reaction scheme, Haber proposed two different routes (direct route and indirect route). In the direct path, nitro groups passed through nitroso and hydroxylamine intermediates to further generate anilines.²⁷ And the indirect route included the condensation of nitroso with hydroxylamine to obtain azoxy compound, which was reduced to azo, hydrazone and aniline compound in a series of continuous steps.²⁸ However, Haber's mechanism was not applicable to all nitroaromatics reduction systems. Visentin proposed a new possible mechanism for reduction of nitroaromatics to anilines according to the calorimetric, FTIR-ATR (attenuated total reflectance), and gas-uptake signals with Pd/C as catalyst.²⁹ In this case, the direct route from nitro compound to hydroxylamine was included in the reaction scheme: nitro → hydroxylamine → aniline.³⁰

In this work, we studied the effect of ruthenium supported on rutile and anatase TiO₂ on the catalytic performance of 4-nitroacetophenone at normal temperature and atmospheric hydrogen. Further studies showed that the crystalline form of TiO₂ had a great influence on the reaction, which was reflected in the transformation route of 4-nitroacetophenone. *In situ* FT-IR data and the experiments proved that the reduction of 4-nitroacetophenone by Ru/TiO₂(A) catalyst was in accordance with the Visentin's reaction path. The reduction of 4-nitroacetophenone by Ru/TiO₂(A) catalyst followed the direct hydrogenation route which the 4-aminoacetophenone was the only product from the beginning to the end of the reaction. However, the Ru/TiO₂(R) causes a series of intermediates accumulation during the conversion process and 4-aminoacetophenone was obtained through the condensation route of hydroxylamine species. It was worth noting that Ru/TiO₂(A) could selectively reduce nitro groups when nitroaromatics contained other competitive reducible groups, proving its excellent applicability.

Experimental section

Materials

High purity nitroaromatics, anhydrous ruthenium trichloride (ruthenium content 45-55%) and nano-titanium dioxide (anatase, 99.8%, 10-20 nm) were purchased from Aladdin Reagent Network. Nano-titanium (IV) oxide (rutile, 0.9-1.6 μm, 99.99%) was purchased from Alfa Aesar Reagent Network. Sodium hydroxide (AR) was purchased from Tianjin Kermel Chemical Reagent Network. Methanol (99.5%) was purchased from Sinopharm Chemical Reagent Co. Ltd.

Preparation of Catalysts

The ruthenium catalyst supported on titanium dioxide was prepared by the impregnation method. RuCl₃ with the required amounts was dissolved in 60 mL ultrapure water to obtain aqueous RuCl₃ solution. Then nano-titanium dioxide (2.0 g) was added and stirred vigorously for 2 h at 25 °C. Water was evaporated under 80 °C until dryness and then the NaOH solution (30 mL) was added to adjust the pH of the solution to 13.2. The final suspension was stirred for 24 h at 25 °C. Next, the mixture was separated by centrifugation, washed by a large amount of water to neutral, and then dried at 60 °C in a vacuum oven for 12 h. Finally, the dried solids were reduced with H₂ for 2 h at 200 °C in a tubular furnace. The Ru nanoparticle was prepared by the same method without adding TiO₂. The anatase and rutile TiO₂ supported Ru catalysts were designated as Ru/TiO₂(A) and Ru/TiO₂(R), respectively.

Characterisation

The powder X-ray diffraction (XRD) patterns were performed on MiniFlex II diffractometer, which were irradiated with Cu Kα1 (λ = 1.5418 Å). High resolution TEM (HRTEM) images were acquired at accelerating voltage 200 kV on a JEM-2100F transmission electron microscope. Raman spectra were measured on a Jobin Yvon HR-800 spectrometer equipped with a 514 nm laser. X-ray photoelectron spectra were recorded by thermal ESCALAB 250 spectrometer (Al Kα source, *hν* = 1486.6 eV). The detailed Ru XPS analysis data of Ru/TiO₂(A) and Ru/TiO₂(R) catalysts as see in supporting information (Table S1).

Pulsed hydrogen adsorption and temperature programmed desorption (TPD)

100 mg catalysts were pretreated for 3 hours in N₂ flow (25 mL min⁻¹) at 300 °C, and then cooled to 55 °C. After the pretreatment, H₂ was injected into the sample by pulse injection for 10-20 min until the adsorption was saturated. After adsorption by pulsed H₂, the system was purged with N₂ flow (25 mL min⁻¹) until the signal was stable. The temperature was raised from 30 to 900 °C (5 °C min⁻¹) with 25 mL min⁻¹ of velocity of argon flow.

In situ diffuse reflection Fourier transform infrared (FT-IR) measurement

Catalyst powder was placed in an *in situ* infrared cell. The reactor has several gas inlets for the introduction of Ar or H₂/Ar and one outlet for the exhaust. Gas flow was controlled by mass flow controllers. *In situ* FT-IR measurements were carried out on Bruker Tensor II infrared spectrometer with a resolution of 4 cm⁻¹. The sample was heated to 100 °C at 5 °C min⁻¹ with a flow rate of 30 mL min⁻¹ in Ar atmosphere, kept 2 hours at 100 °C, and then cooled to 55 °C. 4-nitroacetophenone was introduced into the catalyst sample, and then Ar was used to sweep the sample pool again until a stable spectral signal was obtained. The airbag containing H₂ was introduced into the *in situ* tank slowly through the intake port and the infrared spectra were recorded.

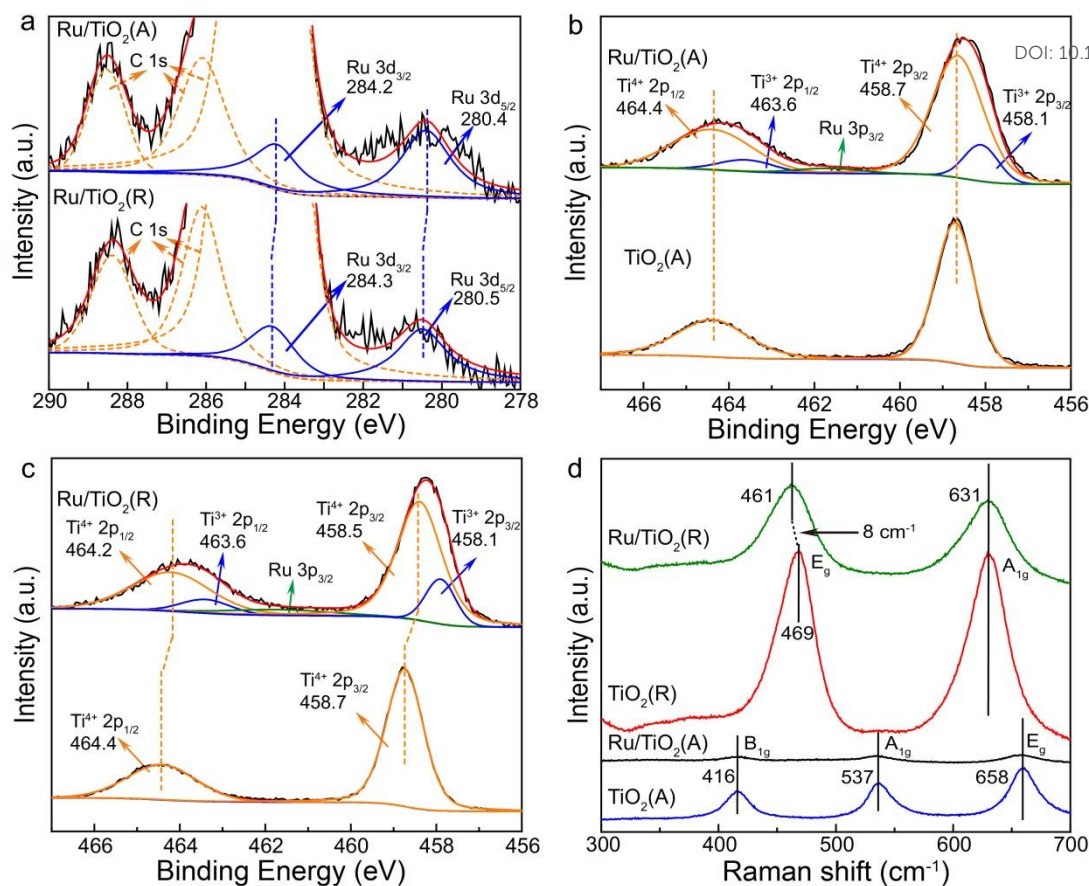


Fig. 1 (a) XPS profiles of Ru species in the Ru/TiO₂(A) and Ru/TiO₂(R) catalysts. (b) XPS profiles of Ti species in the Ru/TiO₂(A) and TiO₂(A) catalysts. (c) XPS profiles of Ti species in the Ru/TiO₂(R) and TiO₂(R) catalysts. (d) Raman spectra of Ru/TiO₂(R), TiO₂(R), Ru/TiO₂(A) and TiO₂(A) catalysts.

Catalytic performance evaluation

10 mg of catalyst, 0.1 mmol of 4-nitroacetophenone, and 2 mL of solvent were added to a 10 mL glass reaction flask. Then atmospheric hydrogen was introduced into the reaction bottle to exhaust the air in the reaction bottle. The bottle must be sealed to guarantee atmospheric hydrogen. The vial was placed in an oil bath to react at the specific temperature. After the reaction, qualitative and quantitative analysis of reactants and products were carried out by high-performance liquid chromatography (HPLC) (Agilent 1260-C18 column). The conversion rate was calculated based on the amount of nitroaromatics.

Results and discussion

The interaction between Ru metal and TiO₂ supports. In order to have a clear understanding of the crystal structure of Ru/TiO₂(A) and Ru/TiO₂(R) catalysts, the structural characteristics were characterised by different microscopic and spectral methods. Fig S1 illustrated the X-ray diffraction (XRD) patterns of Ru/TiO₂(A) and Ru/TiO₂(R) catalysts. It can be seen that the loading of Ru nanoparticles does not affect the crystal structure of TiO₂ and no Ru diffraction peaks are

observed in Ru/TiO₂(A) and Ru/TiO₂(R) catalysts. This may be due to the high dispersion of Ru on the supports. Fig. S2a and Fig. S2b showed the transmission electron microscopic images (TEM) of Ru/TiO₂(A) and Ru/TiO₂(R) catalysts, the Ru nanoparticles were uniformly distributed on the surface of TiO₂. The lattice fringe spacing of 0.214 nm corresponds to the interplanar distance of Ru metal (002) planes (Fig. S2c and Fig. S2d). In addition, Fig. S2e and Fig. S2f showed that the average particle size of Ru nanoparticles were 1.6 nm and 2.4 nm in Ru/TiO₂(A) and Ru/TiO₂(R) catalysts, respectively. The X-ray photoelectron spectroscopy (XPS) analysis of Ru/TiO₂(A) catalysts were provided in Fig. 1a. The binding energies of Ru 3d_{5/2} and Ru 3d_{3/2} at 280.4 and 284.2 eV, respectively, could be attributed to the zero valence state of Ru.³¹ And the binding energies at 464.4 and 458.7 eV were assigned to Ti 2p_{1/2} and Ti 2p_{3/2} of Ti⁴⁺, respectively (Fig. 1b). The spin-orbital splitting was 5.7 eV, which was greatly consistent with the expected value of Ti⁴⁺ oxidation state in titanium dioxide nanocomposites.³² By comparing the Ru/TiO₂(A) catalyst with the pure TiO₂(A), we detected the other two peaks at 463.6 and 458.1 eV which could be classified as Ti 2p_{1/2} and Ti 2p_{3/2} of Ti³⁺ state.³³ This indicated that electrons transfer occurs between Ru and TiO₂(A), resulting in electron deficiency on the surface of the Ru and the formation of Ti³⁺ on the surface of the TiO₂(A).³⁴

And preceding literature also involve in the electrons transfer from Ru to Ti, this may be because the electron of Ru atoms cannot withstand the large attraction from Ti atoms.³⁵ Different crystal of TiO₂ had different ability to attract the electrons. By comparing the Ru/TiO₂(R) with the Ru/TiO₂(A) catalyst, the binding energies of Ru of Ru/TiO₂(R) catalysts were higher for 0.1 eV than that of the Ru/TiO₂(A) catalyst. Compared with TiO₂(R), the binding energies of Ti⁴⁺ of Ru/TiO₂(R) catalysts were moved to the lower binding energy by 0.2 eV, and we also detected a large amount of Ti³⁺ (Fig. 1c). Therefore, compared with TiO₂(A), TiO₂(R) got more electrons from Ru. It was because the concentration of unsaturated Ti cations of anatase was less and the reduction rate was slower than that of rutile.^{36, 37} These observations were consistent with density functional theory (DFT) calculations, which showed that the formation energy of oxygen vacancy (V_o) on rutile was lower than that on anatase.^{38, 39} Therefore, TiO₂(R) was easier to get electrons from Ru and then Ti⁴⁺ was reduced to Ti³⁺.⁴⁰

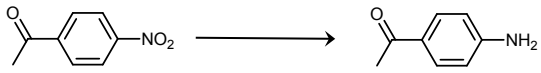
The interaction between Ru and TiO₂ was further verified by Raman spectroscopy (Fig. 1d). Typical Raman bands caused by TiO₂(R) occur at 469 and 631 cm⁻¹, which can be attributed to the E_g (plane O-O vibration) and A_{1g} (Ti-O stretch) modes of rutile phase, respectively.⁴¹ Deposition of Ru species on the surface of TiO₂(R) resulted in a red shift of about 8 cm⁻¹ for E_g mode, which showed the modification of the planar O-O vibration and the formation of Ru-O-Ti bond. While the similar phenomenon did not occur in Ru/TiO₂(A) catalyst. The observed frequency shift was consistent with the results reported by Hong Zhong.⁴² The obvious red shift indicated that there was a strong interaction between Ru and TiO₂(R), which was beneficial for the electrons transfer from Ru nanoparticles to TiO₂(R). Therefore, there were more Ti³⁺ species on the surface of Ru/TiO₂(R).

The hydrogenation depth and chemoselectivity controlled by TiO₂ phases. Anatase and rutile crystals were the most common types of TiO₂. In order to investigate the influence of the crystal phase of TiO₂ on the catalytic performance, we tested the performance of Ru/TiO₂(A) and Ru/TiO₂(R) catalysts under the same experimental conditions. As can be seen from Table 1, the catalytic performance of Ru/TiO₂(A) changed obviously with the increase of Ru loading. The results showed that the Ru/TiO₂(A) catalyst with 2.7 wt% Ru loading exhibited the highest activity for the hydrogenation of 4-nitroacetophenone with H₂ (1 atm) at 55 °C (Table 1, entries 1-4). 99.9% of 4-nitroacetophenone was consumed in 2 h with 99.9% selectivity for 4-aminoacetophenone (Table 1, entry 5). In contrast, 2.7 wt% Ru/TiO₂(R) catalysts gave 99% conversion of 4-nitroacetophenone with a selectivity of 83.5% for 4-aminoacetophenone (Table 1, entry 6). The results showed that the crystal phase of TiO₂ may affect the reduction pathway of 4-nitroacetophenone. Thus, the kinetic experiments for the reduction of 4-nitroacetophenone over Ru/TiO₂(A) and Ru/TiO₂(R) were performed (Fig. 2). When Ru/TiO₂(A) catalyst was used, the selectivity for 4-aminoacetophenone was closed to 99.9% from the initial stage

of the reaction and remained at 99.9% until the reaction was completed. On the contrary, when

DOI: 10.1039/C9CY02260K

Table 1 Catalytic performance of Ru catalyst for conversion of 4-nitroacetophenone to 4-aminoacetophenone.^a



Entry	Catalyst	Time (h)	Conv. (%)	Sel. (%)
1	1.0 wt% Ru/TiO ₂ (A)	1	65.6	99.9
2	2.7 wt% Ru/TiO ₂ (A)	1	83.2	99.9
3	4.1 wt% Ru/TiO ₂ (A)	1	45.4	99.9
4	7.0 wt% Ru/TiO ₂ (A)	1	41.9	99.9
5	2.7 wt% Ru/TiO ₂ (A)	2	99.9	99.9
6	2.7 wt% Ru/TiO ₂ (R)	2	99.9	83.5
7 ^b	2.7 wt% Ru/TiO ₂ (A)	2	99.9	99.9
8 ^c	2.7 wt% Ru/TiO ₂ (A)	2	99.9	99.9
9 ^d	2.7 wt% Ru/TiO ₂ (A)	2	99.9	99.9
10	2.7 wt% Ru/TiO ₂ (A)	12	99.9	99.9
11 ^e	2.7 wt% Ru/TiO ₂ (A)	2	Not detected	-
12	TiO ₂ (A)	2	Not detected	-
13	Ru nanoparticle	2	Not detected	-
14 ^f	2.7 wt% Ru/TiO ₂ (A)	12	99.9	97.8
15 ^g	2.7 wt% Ru/TiO ₂ (A)	12	99.9	97.6

^a Reaction conditions: 10 mg catalyst, 0.1 mmol reactant, 2 mL methanol, 55 °C, 1 atm H₂. ^b 75 °C. ^c 95 °C. ^d 115 °C. ^e 1 atm Ar. ^f 25 mg catalyst, 1 g reactant, 10 mL methanol, 5 atm H₂. ^g 25 mg catalyst, 3 g reactant, 10 mL methanol, 10 atm H₂. The conversion was determined by high-performance liquid chromatography (HPLC). Conv. = Conversion. Sel. = Selectivity.

Ru/TiO₂(R) catalyst was used, there was only a small amount of 4-aminoacetophenone in the early reaction stage. The conversion of 4-nitroacetophenone reached 99.9% within 80 min, which was faster than that of Ru/TiO₂(A) catalyst, but the main product were N-(4-acetylphenyl)-hydroxylamine besides 4-aminoacetophenone. The selectivity of N-(4-acetylphenyl)-hydroxylamine reached the maximum at 60 min (57.4%). With the continuation of the reaction, the selectivity of N-(4-acetylphenyl)-hydroxylamine decreased significantly, while the selectivity of 1,2-bis(4-acetylphenyl)-diazene oxide increased slightly, and then 1,2-bis(4-acetylphenyl)-diazene oxide decreased with the increase of 4-aminoacetophenone as the final reduction product. These results indicated that the reduction of 4-nitroacetophenone over Ru/TiO₂(R) occurred by a condensation route presented by Haber while the Ru/TiO₂(A) catalysts did not.⁴³ Therefore, Ru/TiO₂(A) had higher selectivity for 4-aminoacetophenone than Ru/TiO₂(R).

In the control experiment, when the reaction temperature was raised from 55 to 115 °C and the reaction time was prolonged to 12 h, more than 99% selectivity to 4-aminoacetophenone was still attained (Table 1, entries 7-10). This showed that Ru/TiO₂(A) catalyst could perfectly control the synthesis of 4-aminoacetophenone without further hydrogenation of carboxyl group. It was further confirmed by studying the competitive reaction of nitrobenzene and acetophenone at a molar ratio of 1:1. We found that only the aniline was detected in the product, which showed that Ru/TiO₂(A) catalyst had excellently selective reduction of nitro groups (Fig. 3). According

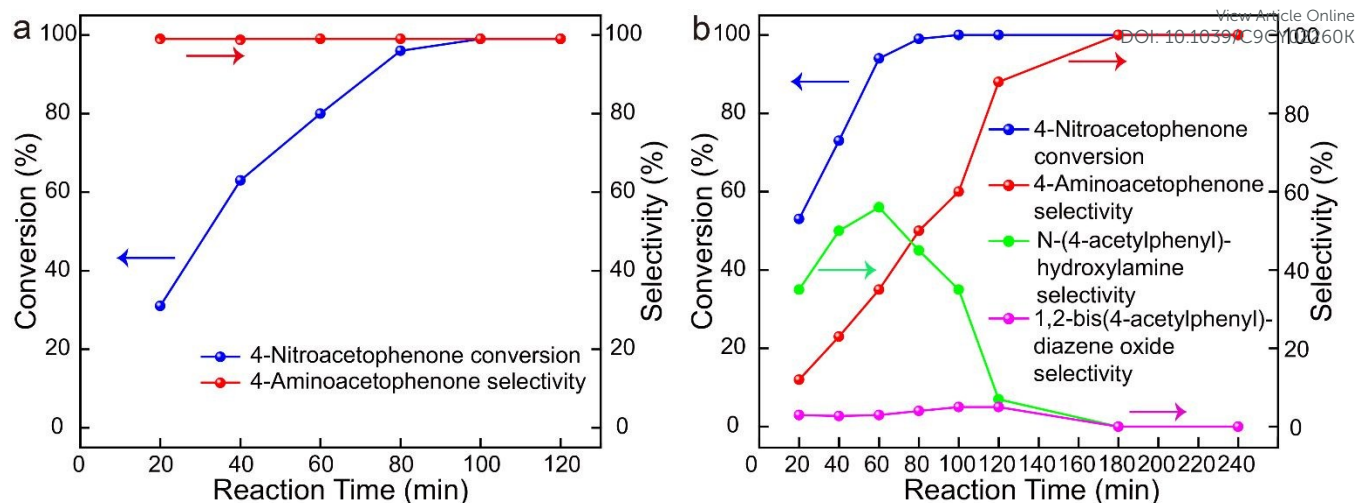


Fig. 2 Time-conversion plots for 4-nitroacetophenone reduction using (a) Ru/TiO₂(A) and (b) Ru/TiO₂(R) as the catalyst. Reaction conditions were identical with Table 1. The conversion was determined by HPLC.

to the literatures, the activation energy for further hydrogenation of 4-aminoacetophenone was higher than that of nitro group reduction in the process of selective hydrogenation of 4-nitroacetophenone.^{9, 12, 44} It was worthy noted that the Ru/TiO₂(A) catalyst thermodynamically allowed catalytic hydrogenation of nitro groups, but was unfavourable for the reduction of carbonyl groups. Therefore, Ru/TiO₂(A) catalyst can control the synthesis of 4-aminoacetophenone without further hydrogenation. When the catalytic hydrogenation of 4-nitroacetophenone over 2.7 wt% Ru/TiO₂(A) was conducted under Ar atmosphere, no 4-nitroacetophenone was converted (Table 1, entry 11). These results suggested that the main hydrogen source for 4-nitroacetophenone reduction in our work was H₂. In addition, TiO₂(A) or unsupported Ru particles did not exhibit any activity for the hydrogenation of 4-nitroacetophenone (Table 1, entries 12 and 13). When the amount of 4-nitroacetophenone was expanded to 1 g, we found that Ru/TiO₂(A) catalyst could still catalyse 4-nitroacetophenone to 4-aminoacetophenone with high conversion (99.9%) and high

conditions were identical with Table 1. The conversion was determined by (HPLC).

selectivity (97.8%) at low pressure (5 atm) (Table 1, entry 14). It is noted that the selectivity to 4-aminoacetophenone remained almost the same at 97.6% when the amount of 4-nitroacetophenone was expanded to 3 g at 10 atm H₂ pressure (Table 1, entry 15).

Activation of nitroacetophenone on TiO₂ surface. In the selective reduction of 4-nitroacetophenone catalysed by Ru/TiO₂ catalyst, the infrared spectrum (IR) clearly reflected the adsorption relation of 4-nitroacetophenone on the surface of the catalysts (Fig. 4). Two different absorption bands appeared at 1534 and 1346 cm⁻¹, which were the asymmetric stretching vibration (ν_{asym}) of the nitro group adsorbed on the surface of Ti-OH group and the symmetric stretching vibration (ν_{sym}) of the nitro group adsorbed on the surface of Ti³⁺.⁴⁵ The strength of (ν_{sym}) band on Ru/TiO₂(R) catalyst was much stronger than that on Ru/TiO₂(A) catalyst, because there were more Ti³⁺ on Ru/TiO₂(R) surface. Yasuhiro et al. also proved that the surface Ti³⁺ atoms were the active site for nitro group hydrogenation.⁴⁶ Therefore, the initial conversion rate of 4-

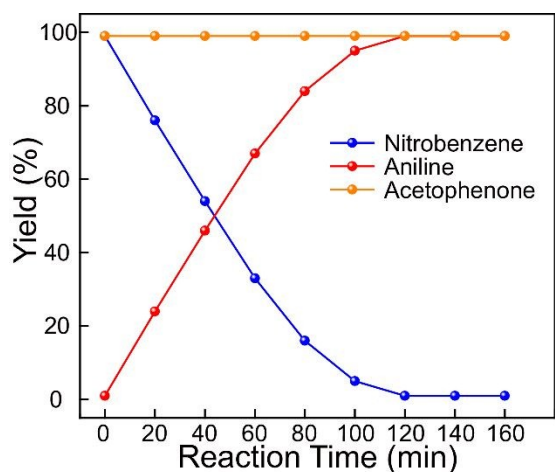
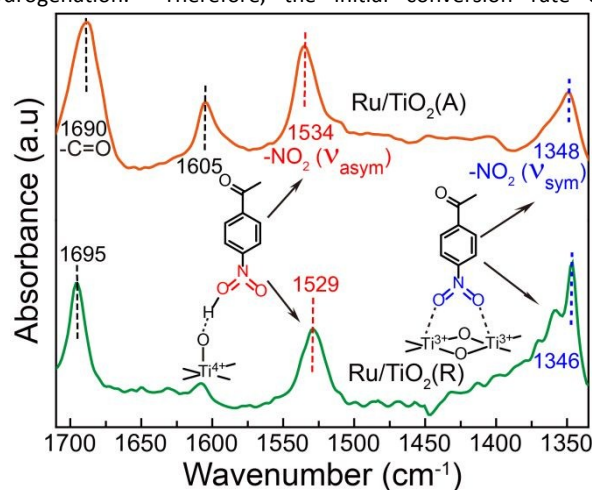


Fig. 3 Time-conversion plots of the mixture of nitrobenzene and acetophenone with a 1:1 molar ratio on Ru/TiO₂(A). Reaction



nitroacetophenone catalysed by Ru/TiO₂(R) was higher than that of Ru/TiO₂(A). Fig. S2 showed the *in situ* FT-IR spectra of 4-nitroacetophenone adsorbed

Fig. 4 *In situ* FT-IR spectra of 4-nitroacetophenone adsorbed on Ru/TiO₂(A) and Ru/TiO₂(R) catalysts. **Table 2** Reaction pathway study of the catalytic performance using Ru/TiO₂(R) and Ru/TiO₂(A) catalysts with various intermediates as substrates.^a

Entry	Reactant	Catalyst	Conv. (%)	Sel. (%)			
				AOB	AB	HAB	AN
1	NSB	Ru/TiO ₂ (R)	99.9	66.1	11.8	4.3	17.8
2 ^b	NSB	Ru/TiO ₂ (R)	99.9	62.3	16.9	0.7	20.1
3	NSB	Ru/TiO ₂ (A)	33.1	99.9	-	-	-
4	PHA	Ru/TiO ₂ (R)	99.9	4.2	18.4	30.3	47.1
5	PHA	Ru/TiO ₂ (A)	99.9	2.7	8.9	-	88.4
6	AOB	Ru/TiO ₂ (R)	99.9	-	7.5	53.2	39.3
7	AOB	Ru/TiO ₂ (A)	43.5	-	42.8	57.2	-

^a Reaction conditions were identical with Table 1. ^b 12 h. The conversion was determined by HPLC. Conv. = Conversion. Sel. = Selectivity. NSB = Nitrosobenzene, PHA = Hydroxylamine, AOB = Azoxybenzene, AB = Azobenzene, HAB = Hydrazobenzene, AN = Aniline.

on the Ru/TiO₂(A) and Ru/TiO₂(R) catalysts, the absorption band at 1636 cm⁻¹ belonged to hydroxyl of water.⁴⁷ In addition, the absorption bands at 1695 and 1653 cm⁻¹ were the C=O stretching vibration ($\nu_{C=O}$) of 4-nitroacetophenone and 4-aminoacetophenone, respectively. The band at 1605 cm⁻¹ belonged to the skeleton vibration peak of the benzene ring.⁴⁸ With the introduction of H₂ stream into Ru/TiO₂(A) (Fig. S3a), the absorption bands at 1695 and 1533 cm⁻¹ decreased and the band at 1653 cm⁻¹ gradually increased. Meanwhile, the characteristic absorption band of 4-aminoacetophenone appeared at 1597 cm⁻¹ was gradually obvious, which was attributed to the NH₂ stretching vibration of 4-aminoacetophenone.⁴⁹ The peak at 1497 cm⁻¹ belonged to the NH-OH vibration peak.⁵⁰ Apart from above bands, obvious characteristic peaks of azoxybenzene (1477 cm⁻¹) and azobenzene (1454 cm⁻¹) were found in the *in situ* FT-IR infrared spectra of Ru/TiO₂(R) catalyst,^{51,52} which further verified the accumulation of azobenzene compounds during the catalytic process (Fig. S3b). In contrast, under the same conditions, no similar *in situ* FT-IR evolution was observed for both pure TiO₂(A) and TiO₂(R) (Fig. S3b).

To clarify the effect of different crystal phase of TiO₂ on the reaction pathway, the reduction of possible intermediates (nitrosobenzene, phenylhydroxylamine and azoxybenzene) were conducted using the Ru/TiO₂(A) and Ru/TiO₂(R) catalysts under the same conditions (Table 2). When Ru/TiO₂(R) was used as catalyst, the conversion of nitrosobenzene was 99.9%. The products included azobenzene, azoxybenzene, hydrazobenzene and aniline (Table 2, entry 1). Therefore, nitroso species seemed to be one of the intermediates in the reduction of 4-nitroacetophenone catalysed by Ru/TiO₂(R) catalysts. However, when the reaction time was prolonged to 12 h, we found that almost no change in the selectivity for 4-aminoacetophenone (Table 2, entry 2). Besides, we have not found nitroso species accumulation in the reaction of 4-nitroacetophenone catalysed by Ru/TiO₂(R) (Fig. 2b), therefore, we have excluded the possibility that nitroso species was the intermediate in the reduction of 4-nitroacetophenone catalysed by Ru/TiO₂(R) catalysts. When Ru/TiO₂(A) catalyst was used, the conversion of nitrosobenzene was only 33.1%, and the product only included azoxybenzene (Table 2, entry 3), so there were no nitroso species in the reduction of 4-nitroacetophenone catalysed by

Ru/TiO₂(A) catalysts. When hydroxylamine was used as a reactant, the conversion of hydroxylamine was 99.9% regardless of which catalyst was used, and the products also included aniline (Table 2, entries 4 and 5). Therefore, hydroxylamine species were the important intermediates both in the reduction of 4-nitroacetophenone catalysed by Ru/TiO₂(R) and Ru/TiO₂(A) catalysts. However, when Ru/TiO₂(R) was used as catalyst, the selectivity of aniline only 47.1% for the conversion of hydroxylamine (Table 2, entry 4), and the selectivity of azobenzene compounds was 52.9%, therefore, hydroxylamines easily generate anilines through the condensation path in the reduction reaction catalysed by Ru/TiO₂(R) catalysts. When azoxybenzene was used as reactant, Ru/TiO₂(R) could achieve 99.9% conversion of azoxybenzene, and the products included azobenzene (7.5%), hydrazobenzene (53.2%) and aniline (39.3%) (Table 2, entry 6). However, the conversion of azoxybenzene catalysed by Ru/TiO₂(A) was only 43.5%, and no aniline was detected (Table 2, entry 7). Based on the above results, it could be concluded that there were no nitroso species and azoxy compounds in the reduction of 4-nitroacetophenone catalysed by Ru/TiO₂(A), because the conversion of nitroso species and azoxy compounds catalysed by Ru/TiO₂(A) catalysts was very slow and the product did not include aniline species. In contrast, when Ru/TiO₂(R) was used as catalyst, azoxybenzene compounds were important intermediates in the reaction.

We propose a reaction pathway to explain this difference, as shown in Fig. S4. The catalytic reduction of 4-nitroacetophenone over Ru/TiO₂(R) catalyst proceeded via a direct pathway and a condensation pathway. Firstly, 4-nitroacetophenone quickly generates hydroxylamine species in the reaction process, and then 4-aminoacetophenone was mainly obtained by the condensation route from hydroxylamine species. However, when Ru/TiO₂(A) was used as the catalyst, 4-aminoacetophenone was completely generated from 4-nitroacetophenone at the initial stage of the reaction, and no other by-products were detected (Fig. 2), indicating that the reaction pathway over Ru/TiO₂(A) catalyst was not in conformity with the Haber's reaction pathway, but through the fast pathway (nitro → hydroxylamine → aniline) proposed by Visentin et al.^{29,53}

Journal Name

ARTICLE

In order to eliminate the influence of catalyst specific surface area and Ru particle size on the reaction mechanism, we also prepared Ru/TiO₂ catalysts with different specific surface areas (Table S2). We still detected a series of hydroxylamine species and accumulated azoxy compounds from the kinetic experiments for the

View Article Online
DOI: 10.1039/C9CY02260K

Catalysis Science & Technology Accepted Manuscript

Published on 20 January 2020. Downloaded by Boston University on 1/20/2020 12:12:10 PM.

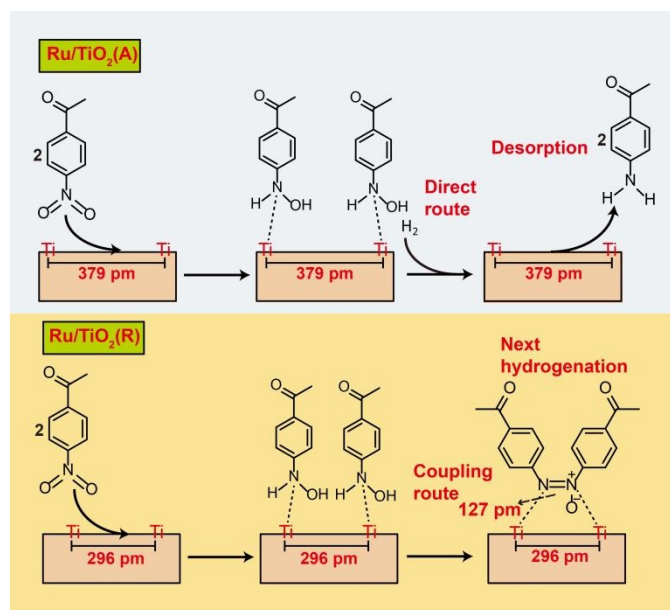


Fig. 5 Plausible catalytic actions of hydroxylamine compound conversion on the surface of TiO_2 .

reduction of 4-nitroacetophenone over the $\text{Ru}/\text{TiO}_2(\text{R}-2)$ catalyst, while the $\text{Ru}/\text{TiO}_2(\text{A}-2)$ allows the highly selective conversion of 4-nitroacetophenone to 4-aminophenone (Fig. S5). Therefore, the specific surface area of the catalyst did not affect the conversion mechanism of 4-nitroacetophenone. We have prepared $\text{Ru}/\text{TiO}_2(\text{A})$ catalysts with ruthenium nano-size of 1.8 and 2.1 nm by controlling the reduction time of Ru catalysts under hydrogen. No accumulation of intermediates has been detected under the same experimental conditions (Table S3 and Fig. S6). Furthermore, we obtained the Ru dispersions of Ru/TiO_2 catalysts based on the pulsed hydrogen adsorption. There was no obvious difference for the Ru dispersions on the TiO_2 support (Table S4, entries 1 and 2). Therefore, in this work, the specific surface area of the catalyst, Ru dispersions and the particle size of Ru had no influence on the reduction mechanism of 4-nitroacetophenone.

For the rutile surface, the distance between two adjacent surface Ti atoms was 296 pm, and that of the anatase was 379 pm (Fig. 5).⁵⁴ Since the actual N=N bond length of azobenzene compound was 127 pm,⁵⁵ in the case of rutile, the reaction intermediate hydroxylamine species were easily coupled to form azoxy compound compared with anatase.^{30, 56, 57} This was why the subsequent conversion efficiency of 4-nitroacetophenone catalysed by $\text{Ru}/\text{TiO}_2(\text{R})$ was poor than that of the $\text{Ru}/\text{TiO}_2(\text{A})$ catalyst.

Activation of H_2 on Ru and H spillover. For the hydrogenation of nitroaromatics, the dissociation of hydrogen was a rate-determining step, thus, effective dissociation of hydrogen by the catalyst can greatly improve the activity of the reaction.⁵⁸ In order to confirm this, a series of $\text{Ru}/\text{TiO}_2(\text{A})$ with different Ru loadings were measured by H_2 pulse adsorption at reaction temperature (Fig. 6a). The saturation adsorption amount of hydrogen on pure $\text{TiO}_2(\text{A})$ was $1 \mu\text{mol g}^{-1}$, while the saturation adsorption amount of hydrogen on 2.7 wt% $\text{Ru}/\text{TiO}_2(\text{A})$ catalyst was $74.7 \mu\text{mol g}^{-1}$, indicating that the loading of metal Ru greatly

improved the saturation adsorption amount of H_2 . At the same time, the hydrogen saturation adsorption capacity of different catalysts had similar trends with the catalytic activity for hydrogenation of 4-nitroacetophenone. Excessive H_2 adsorption on the metal surface also makes it possible for hydrogen spill from the metal surface to the support surface.

The active sites of H_2 adsorption were studied by temperature programmed desorption (TPD). From the H_2 -TPD spectra of $\text{Ru}/\text{TiO}_2(\text{A})$, we can see that there were a small H_2 desorption peak at 37 °C and a large one at 125 °C (Fig. 6b). These results showed that there were at least two H_2 chemisorption sites on the catalyst surface, and the peak at 37 °C was usually attributed to hydrogen adsorbed on Ru metal.⁵⁹ The low desorption temperature indicated that it was a weak chemisorption. The broad peak at 125 °C may be related to the strong chemisorption between hydrogen and the catalyst.⁶⁰ The weak desorption peak near 300 °C were designated as hydrogen desorption from metal onto the surface of the support or hydrogen adsorbed at the interface between the metal and the support.⁶¹

In order to investigate the activation of H_2 on the surface of $\text{Ru}/\text{TiO}_2(\text{A})$ catalyst, the adsorption of H_2 on the surface of catalyst was also measured by *in situ* FT-IR, which further verified the spillover process of H atom on the surface of catalyst. It was found that there was a significant change in the peak as H_2 was flowing into the surface of the catalyst. The peaks at 1889, 1942, 1967 and 1991 cm^{-1} belonged to Ru-H stretching vibration peak ($\nu_{\text{Ru-H}}$) (Fig. 6c).⁶² With the introduction of H_2 , the intensity of these peaks first increased and then decreased, which indicated that hydrogen atoms were formed on Ru and then spilled over onto the support. And the stretching vibration peaks at 1617 and 1636 cm^{-1} gradually increased which can be attributed to O-H stretching vibration

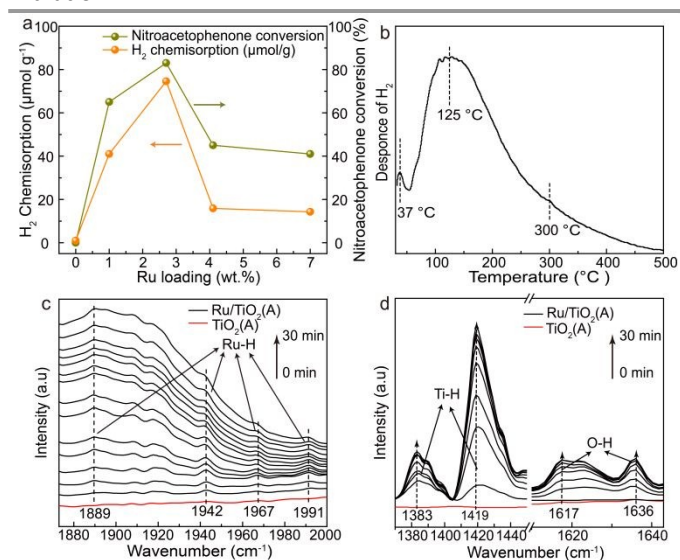
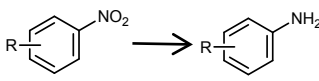
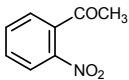
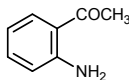
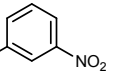
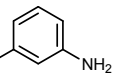
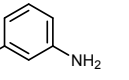
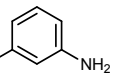
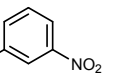
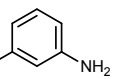
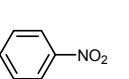
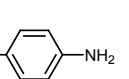
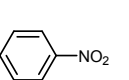
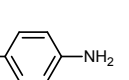
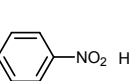
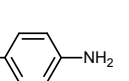
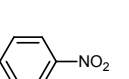
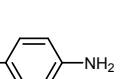
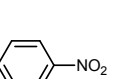
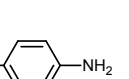
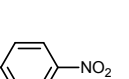
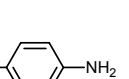
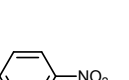
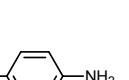
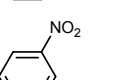
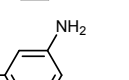


Fig. 6 (a) Dependencies of H_2 chemisorption capacity and 4-nitroacetophenone conversion of different Ru loadings in $\text{TiO}_2(\text{A})$ -supported catalysts. (b) H_2 -TPD profiles of $\text{Ru}/\text{TiO}_2(\text{A})$. (c, d) The *in situ* FT-IR spectra of H_2 adsorbed on $\text{TiO}_2(\text{A})$ and $\text{Ru}/\text{TiO}_2(\text{A})$ catalyst in a flow of H_2 at 55 °C.

Table 3 Catalytic reduction of substituted nitroaromatics using the Ru/TiO₂(A) catalyst.^a

Entry	Reactant	Product	Conv. (%)	Sel. (%)
				
1			99.9	99.9
2			99.9	99.9
3			99.9	99.9
4			99.9	99.9
5			99.9	99.9
6			99.9	99.9
7			99.9	99.9
8			99.9	99.9
9			99.9	99.9
10 ^b			99.9	98.5
11 ^b			99.9	97.1
12 ^b			99.9	95.3

^a Reaction conditions were identical with Table 1. ^b 1.5 h. The conversion were determined by HPLC. Conv. = Conversion, Sel. = Selectivity.

($\nu_{\text{O-H}}$) (Fig. 6d).⁶³ Meanwhile, the peaks of 1393 and 1419 cm⁻¹ became more and more clear which belonged to the Ti-H stretching vibration peaks ($\nu_{\text{Ti-H}}$).⁶⁴ However, the vibration peaks of these bonds were not observed *in situ* FT-IR of pure TiO₂(A).

Combined with the peaks of $\nu_{\text{O-H}}$, $\nu_{\text{Ti-H}}$ and $\nu_{\text{Ru-H}}$ observed during the adsorption process,

DOI: 10.1039/C9CY02260K

it can be concluded that H₂ can dissociate on the Ru surface and then

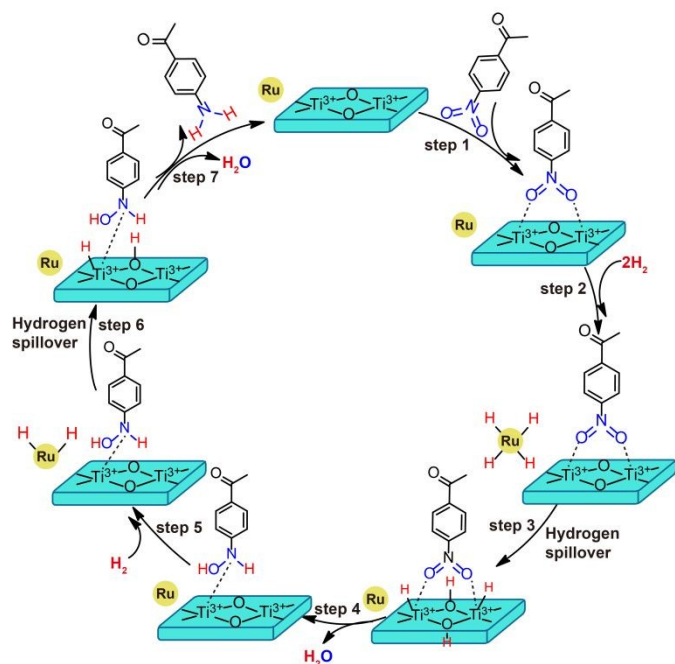
spill over to the TiO₂(A) surface. These spillover hydrogen species combined with surface oxygen atoms and titanium atoms formed O-H and Ti-H bonds, and then reacted with nitro groups which were adsorbed on TiO₂(A) support, showing excellently catalytic performance of the catalyst.

The generality and recyclability of Ru/TiO₂(A). The reusability of the catalyst was an important indicator for testing the performance of the catalyst. We separated and dried the used Ru/TiO₂(A) catalyst and reused it five times under the same reaction conditions. The results showed that the reused Ru/TiO₂(A) catalyst had no obvious change in activity and selectivity, proving its excellent stability and repeatability (Fig. S7).

To explore the applicability of the Ru/TiO₂(A) catalyst, a series of substituted nitroarenes were used to verify its activity under optimized conditions (Table 3). It was found that these substituted nitroarenes containing other reducing functional groups can generate corresponding amino derivatives with high efficiency and high selectivity over Ru/TiO₂(A) catalyst. Both 2-nitroacetophenone and 3-nitroacetophenone could be selectively reduced to the corresponding aminoacetophenone, which showed that steric hindrance did not affect the selectivity of the catalyst. At the same time, 4-halonitrobenzene containing halogen (F, Cl) also had no obvious dehalogenation phenomenon in the reaction process. In particular, nitroaromatics with some sensitive -CN, -CHO and -COOH substituents were also selectively converted into corresponding amino compounds. Especially, nitrobenzene derivatives containing C=C and C≡C can also selectively reduce nitro, but keep the C=C and C≡C unchanged. These results showed that Ru/TiO₂(A) catalyst had universal applicability for hydrogenation of different nitroarenes to anilines with atmospheric H₂.

Proposed mechanism. Ru/TiO₂(A) exhibited high activity and selectivity in the reduction of 4-nitroacetophenone to 4-aminoacetophenone, which may be beneficial from the strong interaction between TiO₂ support and Ru metal. Electrons were transferred from Ru metal into the TiO₂ surface to form Ti³⁺ species which were conducive to the polarization of nitro groups adsorbed on the surface of the support, thus making the N=O bond more vulnerable to hydrogen attack. Moreover, Ru had an excellent ability to adsorb H₂, which make it possible for H spillover from the Ru nanoparticles onto the surface of TiO₂. Therefore, we proposed such a reaction mechanism to explain this phenomenon (Scheme 1). Firstly, nitro groups were adsorbed on the Ti³⁺ sites on the surface of Ru/TiO₂(A) catalysts by symmetric stretching vibration (step 1). Secondly, hydrogen was dissociated under the activation of Ru metal to form Ru-H bond (step 2). Thirdly, the hydrogen atoms on the surface of Ru metal spilled to the TiO₂(A) support to form O-H and Ti-H bonds (step 3). Subsequently, O-H and Ti-H bonds reacted with nitro groups which was adsorbed on the surface of Ru/TiO₂(A) to produce hydroxylamine intermediates (step 4),

and hydroxylamine intermediates were adsorbed on the surface of $\text{TiO}_2(\text{A})$ through nitrogen atoms⁶⁵. Then the hydrogen



Scheme 1 Possible mechanism of 4-nitroacetophenone conversion catalysed by $\text{Ru}/\text{TiO}_2(\text{A})$ catalysts.

dissociated under the site of Ru and spilled onto the $\text{TiO}_2(\text{A})$ support to form O-H and Ti-H bonds repeatedly (steps 5-6). Finally, hydroxylamine was further hydrogenated and dehydrated to produce 4-aminoacetophenone. 4-aminoacetophenone did not undergo any further hydrogenation reaction and then desorbed from the surface of the support (step 7).

Conclusions

Ru/TiO_2 catalysts can selectively reduce 4-nitroacetophenone to 4-aminoacetophenone at normal temperature and atmospheric hydrogen. When $\text{Ru}/\text{TiO}_2(\text{R})$ was used as catalyst, 4-nitroacetophenone was reduced via a direct pathway and a condensation pathway. However, the reduction of 4-nitroacetophenone over $\text{Ru}/\text{TiO}_2(\text{A})$ occurs by direct hydrogenation route proposed by Visentin. The results suggested that the crystal forms of TiO_2 changed the reduction pathway of 4-nitroacetophenone, which was attributed to the relationship between the distance of two adjacent Ti atoms of TiO_2 surface and the bond length of $\text{N}=\text{N}$. Compared with the bond length of $\text{N}=\text{N}$, the distance of Ti-Ti on anatase surface was much bigger than that on the rutile surface, so hydroxylamine intermediate adsorbed on Ti of anatase surface was difficult to form azo oxide species through the condensation route, avoiding the accumulation of azo oxide species. Furthermore, 99.9% conversion with a selectivity of 99.9% to 4-aminoacetophenone was obtained by the reduction of 4-nitroacetophenone over 2.7 wt% $\text{Ru}/\text{TiO}_2(\text{A})$

catalyst. Moreover, $\text{Ru}/\text{TiO}_2(\text{A})$ also exhibited excellent stability and repeatability. In addition, $\text{Ru}/\text{TiO}_2(\text{A})$ can achieve chemoselectivity reduction of nitroaromatics to corresponding anilines in the presence of -CN, -CHO, -COOH, $\text{C}=\text{C}$ and $\text{C}\equiv\text{C}$. The excellent catalytic performance derives from the synergistic effect between TiO_2 and Ru: nitro groups were effectively adsorbed on the surface of TiO_2 ; electrons were transferred from Ru metal into the TiO_2 surface to form Ti^{3+} species, which were conducive to the polarization of nitro groups adsorbed on the surface of the support, thus making the $\text{N}=\text{O}$ bond more vulnerable to hydrogen attack; hydrogen was dissociated on the surface of Ru, then hydrogen atoms spilled onto the surface of TiO_2 to form Ti-H and O-H bond, and further reacted with 4-nitroacetophenone to generate 4-aminoacetophenone.

Conflicts of interest

There are no conflicts to declare.

Acknowledgements

We appreciate the financial support from the National Natural Science Foundation of China (No. 21773284) and the Hundred Talents Program of the Chinese Academy of Sciences and Shanxi Province.

Notes and references

1. M. Shokouhimehr, K. Hong, T. H. Lee, C. W. Moon, S. P. Hong, K. Zhang, J. M. Suh, K. S. Choi, R. S. Varma and H. W. Jang, *Green Chem.*, 2018, **20**, 3809-3817.
2. N. Daems, J. Wouters, C. V. Goethem, K. Baert, C. Poleunis, A. Delcorte, A. Hubin, I. F. J. Vankelecom and P. P. Pescarmona, *Appl. Catal. B*, 2018, **226**, 509-52.
3. S. Doherty, J. G. Knight, T. Backhouse, R. J. Summers, E. Abood, W. Simpson, W. Paget, R. A. Bourne, T. W. Chamberlain, R. Stones, K. R. J. Lovelock, J. M. Seymour, M. A. Isaacs, C. Hardacre, H. Daly and N. H. Rees, *ACS Catal.*, 2019, **9**, 4777-4791.
4. Y. Tan, X. Y. Liu, L. Zhang, A. Wang, L. Li, X. Pan, S. Miao, M. Haruta, H. Wei, H. Wang, F. Wang, X. Wang and T. Zhang, *Angew. Chem., Int. Ed.*, 2017, **56**, 2709-2713.
5. J. Mao, W. Chen, W. Sun, Z. Chen, J. Pei, D. He, C. Lv, D. Wang and Y. Li, *Angew. Chem., Int. Ed.*, 2017, **56**, 11971-11975.
6. J. Wang, Z. Ge, L. Pei, P. Kong, R. Wang, P. Zhu, M. Liu, X. Gu and Z. Zheng, *Catal. Sci. Technol.*, 2019, **9**, 6681-6690.
7. N. Daems, F. Risplendi, K. Baert, A. Hubin, I. F. J. Vankelecom, G. Cicero and P. P. Pescarmona, *J. Mater. Chem. A*, 2018, **6**, 13397-13411.
8. A. Corma and P. Serna, *Science*, 2006, **313**, 332-334.
9. K. Currall and S. D. Jackson, *Appl. Catal. A*, 2014, **484**, 59-63.
10. P. Serna and A. Corma, *ACS Catal.*, 2015, **5**, 7114-7121.
11. J. M. Hawkins and T. W. Makowski, *Org. Process Res. Dev.*, 2001, **5**, 328-330.
12. M. I. A. Wahab and S. D. Jackson, *Appl. Catal. A*, 2013, **462-463**, 121-128.
13. X. Yin, D. He, P. Jiang, G. Zhou, H. Chen and Y. Deng, *Appl. Catal. A*, 2016, **509**, 38-44.
14. A. Corma, P. Serna, P. Concepcion and J. J. Calvino, *J. Am. Chem. Soc.*, 2008, **130**, 8748-8753.

15. Y. Shiraishi, H. Hirakawa, Y. Togawa, Y. Sugano, S. Ichikawa and T. Hirai, *ACS Catal.*, 2013, **3**, 2318-2326.
16. K. Kimura, S. Naya, Y. Jin and H. Tada, *J. Phys. Chem. C*, 2012, **116**, 7111-7117.
17. K. A. Connelly and H. Idriss, *Green Chem.*, 2012, **14**, 260-280.
18. G. S. Herman, Z. Dohnalek, N. Ruzycski and U. Diebold, *J. Phys. Chem. B*, 2003, **107**, 2788-2795.
19. S. Challagulla, K. Tarafder, R. Ganesan and S. Roy, *Sci. Rep.*, 2017, **7**, 8783.
20. T. Omotoso, S. Boonyasuwat and S. P. Crossley, *Green Chem.*, 2014, **16**, 645-652.
21. A. Kim, C. Sanchez, G. Patriarche, O. Ersen, S. Moldovan, A. Wisnet, C. Sassoeye and D. P. Debecker, *Catal. Sci. Technol.*, 2016, **6**, 8117-8128.
22. X. Chen, L. Liu and F. Huang, *Chem. Soc. Rev.*, 2015, **44**, 1861-1885.
23. A. Grirrane, A. Corma and H. García, *Science*, 2008, **322**, 1661-1663.
24. R. V. Jagadeesh, A. E. Surkus, H. Junge, M. M. Pohl, J. Radnik, J. Rabeah, H. Huan, V. Schunemann, A. Bruckner and M. Beller, *Science*, 2013, **342**, 1073-1076.
25. F. A. Westerhaus, R. V. Jagadeesh, G. Wienhofer, M. M. Pohl, J. Radnik, A. E. Surkus, J. Rabeah, K. Junge, H. Junge, M. Nielsen, A. Bruckner and M. Beller, *Nat. Chem.*, 2013, **5**, 537-543.
26. A. Noschese, A. Buonerba, P. Canton, S. Milione, C. Capacchione and A. Grassi, *J. Catal.*, 2016, **340**, 30-40.
27. M. Makosch, J. Sá, C. Kartusch, G. Richner, J. A. Bokhoven and K. Hungerbühler, *ChemCatChem*, 2012, **4**, 59-63.
28. X. Guo, C. Hao, G. Jin, H. Y. Zhu and X. Y. Guo, *Angew. Chem., Int. Ed.*, 2014, **53**, 1973-1977.
29. F. Visentin, G. Puxty, O. M. Kut and K. Hungerbu, *Ind. Eng. Chem. Res.*, 2006, **45**, 4544-4553.
30. E. A. Gelder, S. D. Jackson and C. M. Lok, *Chem. Commun.*, 2005, 522-524.
31. R. Berthoud, P. Délichère, D. Gajan, W. Lukens, K. Pelzer, J.-M. Basset, J.-P. Candy and C. Copéret, *J. Catal.*, 2008, **260**, 387-391.
32. S. Nong, W. Dong, J. Yin, B. Dong, Y. Lu, X. Yuan, X. Wang, K. Bu, M. Chen, S. Jiang, L. M. Liu, M. Sui and F. Huang, *J. Am. Chem. Soc.*, 2018, **140**, 5719-5727.
33. Q. Xiao, J. Zhang, C. Xiao, Z. Si and X. Tan, *Sol. Energy*, 2008, **82**, 706-713.
34. D. Tsukamoto, Y. Shiraishi, Y. Sugano, S. Ichikawa, S. Tanaka and T. Hirai, *J. Am. Chem. Soc.*, 2012, **134**, 6309-6315.
35. L. Å. Näslund, C. M. S. Sánchez, Á. S. Ingason, J. Bäckström, E. Herrero, J. Rosen and S. Holmin, *J. Phys. Chem. C*, 2013, **117**, 6126-6135.
36. U. Diebold, J. Lehman, T. Mahmoud, M. Kuhn, W. Hebenstreit, G. Leonardelli, M. Schmid and P. Varga, *Surf. Sci.*, 1998, **411**, 137-153.
37. W. Hebenstreit, N. Ruzycski, G. S. Herman, Y. F. Gao, and U. Diebold, *Phys. Rev. B*, 2000, **62**, 334-336.
38. B. Hudec, K. Hušková, A. Rosová, J. Šoltýs, R. Rammula, A. Kasikov, T. Uustare, M. Mičušík, M. Omastová, J. Aarik and K. Fröhlich, *J. Phys. D: Appl. Phys.*, 2013, **46**, 385304.
39. N. A. Pérez, M. P. Ruiz, J. Echave and J. Faria, *Appl. Catal. A*, 2017, **531**, 106-118.
40. B. Coq, A. Tijani, R. Dutartre and F. Figueras, *J. Mol. Catal.*, 1993, 253-264.
41. Q. Lin, Y. Huang, Y. Wang, L. Li, X. Y. Liu, F. Lv, A. Wang, W.-C. Li and T. Zhang, *J. Mater. Chem. A*, 2014, **2**, 5178-5181.
42. H. Zhong, C. Yang, L. Fan, Z. Fu, X. Yang, X. Wang and R. Wang, *Energy Environ. Sci.*, 2019, **12**, 418-426.
43. Q. Xiao, S. Sarina, E. R. Waclawik, J. Jia, J. Chang, J. D. Riches, H. Wu, Z. Zheng and H. Zhu, *ACS Catal.*, 2016, **6**, 1744-1753.
44. N. Perret, X. Wang, T. Onfroy, C. Calers and M. A. Keane, *J. Catal.*, 2014, **309**, 333-342.
45. I. Ahmad, T. J. Dines, C. H. Rochester and J. A. Anderson, *J. Chem. Soc., Faraday Trans.*, 1996, **92**, 3225-3231.
46. Y. Shiraishi, Y. Togawa, D. Tsukamoto, S. Tanaka and T. Hirai, *ACS Catal.*, 2012, **2**, 2475-2481.
47. B. L. Mojet, S. D. Ebbesen and L. Lefferts, *Chem. Soc. Rev.*, 2010, **39**, 4643-4655.
48. U. Hartfelder, C. Kartusch, J. Sá and J. A. Bokhoven, *Catal. Commun.*, 2012, **27**, 83-87.
49. C. H. Hao, X. N. Guo, M. Sankar, H. Yang, B. Ma, Y. F. Zhang, X. L. Tong, G. Q. Jin and X. Y. Guo, *ACS Appl. Mater. Interfaces*, 2018, **10**, 23029-23036.
50. A. Corma, P. Concepcion and P. Serna, *Angew. Chem., Int. Ed.*, 2007, **46**, 7266-7269.
51. G. Rauhut, A. A. Jarzecki and P. Pulay, *J. Comput. Chem.*, 1997, 489-450.
52. M. M. J. Tecklenburg, D. J. Kosnak, A. Bhatnagar and D. K. Mohanty, *J. Raman. Spectrosc.*, 1997, **28**, 755-763.
53. H.-U. Blaser, *Science*, 2006, **313**, 312-314.
54. Y. Kakuma, A. Y. Nosaka and Y. Nosaka, *Phys. Chem. Chem. Phys.*, 2015, **17**, 18691-18698.
55. J. P. P. Ramalho and F. Illas, *Chem. Phys. Lett.*, 2011, **501**, 379-384.
56. A. S. Mendkovich, M. A. Syroeshkin, D. V. Ranchina, M. N. Mikhailov, V. P. Gulytai and A. I. Rusakov, *J. Electroanal. Chem.*, 2014, **728**, 60-65.
57. A. K. Shil and P. Das, *Green Chem.*, 2013, **15**, 3421.
58. P. Serna, P. Concepción and A. Corma, *J. Catal.*, 2009, **265**, 19-25.
59. H.-Y. Lin and Y.-W. Chen, *Thermochim. Acta.*, 2004, **419**, 283-290.
60. L. Chen, Y. Li, X. Zhang, Q. Zhang, T. Wang and L. Ma, *Appl. Catal. A*, 2014, **478**, 117-128.
61. P. Panagiotopoulou, D. I. Kondarides and X. E. Verykios, *J. Phys. Chem. C*, 2011, **115**, 1220-1230.
62. K. Hashimoto, N. Toukai, *J. Mol. Catal. A: Chem.*, 2000, **161**, 171-178.
63. G. Richner, J. A. Bokhoven, Y. M. Neuhold, M. Makosch and K. Hungerbühler, *Phys. Chem. Chem. Phys.*, 2011, **13**, 12463-12471.
64. G. Wang, Y. Gong, M. Chen and M. Zhou, *J. Am. Chem. Soc.*, 2006, **128**, 5974-5980.
65. L. Wang, E. Guan, J. Zhang, J. Yang, Y. Zhu, Y. Han, M. Yang, C. Cen, G. Fu, B. C. Gates and F. S. Xiao, *Nat. Commun.*, 2018, **9**, 1362.

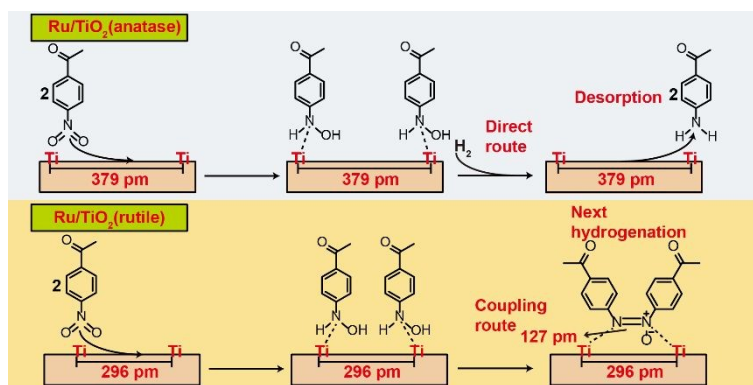
Differences in Selective Reduction Mechanism of 4-Nitroacetophenone Catalyzed by Rutile and Anatase Supported Ruthenium Catalysts

Jin Zhang,^{ab} Linjuan Pei,^{ab} Jie Wang,^{ab} Pengqi Zhu,^{*ab} Xianmo Gu^{*a} and Zhanfeng Zheng^{*ab}

^a State Key Laboratory of Coal Conversion, Institute of Coal Chemistry, Chinese Academy of Sciences, Taiyuan 030001, China.

^b Center of Materials Science and Optoelectronics Engineering, University of Chinese Academy of Sciences, Beijing 100049, China.

* E-mail: zfzheng@sxicc.ac.cn (Z. F. Zheng); guxm@sxicc.ac.cn (X. M. Gu); zhupengqi15@mails.ucas.ac.cn (P. Q. Zhu).



Ru nanoparticles supported on different crystalline TiO₂(anatase and rutile) result in different reaction pathways for 4-nitroacetophenone.